

Polarization dependence of the ϕ meson mass from finite-temperature QCD sum rules

Hidefumi Matsuda*

Zhejiang Institute of Modern Physics, Department of Physics, Zhejiang University, Hangzhou, 310027, China

Philipp Gubler†

Advanced Science Research Center, Japan Atomic Energy Agency, Tokai, Ibaraki 319-1195, Japan

Koichi Hattori‡

*Zhejiang Institute of Modern Physics, Department of Physics,
Zhejiang University, Hangzhou, 310027, China and*

Research Center for Nuclear Physics (RCNP), Osaka University, Osaka 567-0047, Japan

We study the ϕ meson at finite temperature and finite momentum using QCD sum rules. The presence of medium breaks the Lorentz invariance, and induces distinct in-medium modifications of the transverse and longitudinal modes at finite momentum. We find that, with increasing momentum, the masses of both modes increase and a clear transverse–longitudinal splitting develops. The splitting is found to grow with temperature and to be mainly generated by the dimension-four spin-dependent thermal condensates.

I. INTRODUCTION

In-medium effects on vector mesons serve as a useful experimental probe of the low-temperature and low-to-intermediate-density region of the QCD phase diagram. On the timescale of hadronic matter created in collision experiments, vector mesons are better regarded as finite-lifetime impurities propagating through the medium rather than as particles fully equilibrated with it. Their properties are expected to be modified by interactions with the surrounding hadronic environment. Such in-medium modifications of vector meson properties can reflect essential features of the hadronic regime of the QCD phase diagram, such as the partial restoration of chiral symmetry, medium-induced hadronic excitations, and temperature- and density-dependent changes in the dominant hadronic degrees of freedom of the medium.

The ϕ meson occupies a special position among light vector mesons since its quark content is close to a pure $s\bar{s}$ state [1], and its in-medium properties are strongly influenced by strange hadronic channels, especially the $K\bar{K}$ channel. It therefore provides information complementary to that obtained from the ρ and ω mesons. Experimental measurements and related analyses at various facilities have provided evidence for in-medium modifications of the ϕ meson properties, in particular those induced by finite-density effects [2–9]. While these studies have mainly addressed finite-density effects, the focus has more recently extended to regimes where finite-temperature effects also become important. Ongoing and planned experimental programs, such as J-PARC-HI, CBM at FAIR, MPD at NICA, and CEE at HIRFL-CSR, aim to explore such regimes of the QCD phase diagram.

Theoretical studies of ϕ meson properties at finite temperature have a long history. Important results have been obtained from QCD sum rules [10, 11] as well as from hadronic effective-model approaches which include effects of fluctuations in relevant hadronic channels, such as $K\bar{K}$ and $\pi\rho$, and scattering processes with thermal hadrons in the medium [12–18]. It is challenging, in particular, for lattice QCD simulations because extracting the real-time spectral information at finite temperature requires analytic continuation from the imaginary-time formalism, even at zero chemical potential where the fermion sign problem does not arise.

The meson properties depend not only on temperature but also on momentum because of the existence of a preferred Lorentz frame, i.e., a medium rest frame. Understanding the momentum dependence is important for phenomenological applications to the aforementioned experiments. Furthermore, the absence of Lorentz invariance implies that the longitudinal and transverse modes with respect to a vector-meson momentum can receive different modifications at finite momentum. As finite-temperature regimes become experimentally accessible and precision in experimental measurements is improved, this effect is becoming increasingly relevant [19, 20]. Investigating the thermal origin of the longitudinal-transverse splitting of the finite-momentum ϕ meson is therefore a timely theoretical task, also in light of the recent measurements of the ϕ meson polarization in non-central heavy-ion collisions [21, 22], for which the polarization dependence considered in this work could be relevant.

In this paper, we study the in-medium properties of the ϕ meson in the low-temperature hadronic phase at vanishing baryon number using QCD sum rules [23, 24] as a nonperturbative method complementary to lattice QCD simulations. Our main focus is the longitudinal-transverse splitting of the ϕ meson at finite momentum, and we systematically investigate its temperature and

* da.matsu.00.bbb.kobe@gmail.com

† gubler.philipp@jaea.go.jp; philipp.gubler1@gmail.com

‡ koichi.hattori@zju.edu.cn

momentum dependence. The QCD sum rules has been successfully applied to the ϕ meson in vacuum [24] and in medium [10, 11, 25–28]. We include the non-scalar condensates up to dimension six in the OPE following Ref. [29], capturing both the leading ($d = 4$) and subleading ($d = 6$) contributions to the splitting. We evaluate the non-scalar condensates, which are purely medium-induced contributions, using the dilute pion gas approximation [30]. This is justified because pions are the relevant degrees of freedom in our target temperature range. With these ingredients, we identify the non-scalar condensates responsible for it.

This paper is organized as follows. In Sec. II, we introduce the basic framework of QCD sum rules and the explicit setup used in the present analysis. In Sec. III, we present numerical results for the ϕ meson properties at finite temperature. In Sec. IV, we summarize our findings.

II. QCD SUM RULES

In this section, we first recaptulate basics of QCD sum rules applied to finite temperature and the OPE developed in Ref. [29]. Then, we evaluate the relevant condensates at finite temperature in the subsections after Sec. II C. We also summarize the phenomenological modeling of the spectral function and the Borel transformation for the numerical analysis performed in the result section.

A. Basic idea of the QCD sum rule

QCD sum rules are a QCD-based approach to extracting hadronic spectral information from two-point correlation functions. This approach relies on a dispersion relation connecting the correlation function to an integral of the spectral function over the invariant mass. The correlator is evaluated at deep spacelike momenta using the OPE, while the spectral function is parametrized phenomenologically (see, however, Refs.[31, 32] for attempts without explicit parametrizations). In this sense, the dispersion relation serves as a bridge between the QCD side, where the short-distance physics is encoded in the OPE, and the hadronic side, where the long-distance physics is represented by the spectral function. The model parameters, such as the hadron mass and hadron decay width, are then determined by requiring consistency between the two sides of the dispersion relation.

The present analysis for the ϕ meson is based on the thermal current correlator

$$\Pi^{\mu\nu}(q, T) = i \int d^4x e^{iq \cdot x} \langle \mathcal{T} J^\mu(x) J^\nu(0) \rangle_T, \quad (1)$$

where $J^\mu = \bar{s} \gamma^\mu s$ is the strange vector current and $\langle \dots \rangle_T$ denotes the thermal average. The correlator $\Pi^{\mu\nu}$ is symmetric and, by the Ward identity, transverse to the four-

momentum: $q_\mu \Pi^{\mu\nu} = 0$. In vacuum, the only available symmetric second-rank tensors are $q^\mu q^\nu$ and $g^{\mu\nu}$, and these conditions reduce $\Pi^{\mu\nu}$ to a single scalar amplitude, $\Pi^{\mu\nu} = P^{\mu\nu} \Pi^{\text{vac}}$ where $P^{\mu\nu} = q^\mu q^\nu - q^2 g^{\mu\nu}$. At finite temperature, there is a timelike vector u^μ , of which the spatial component specifies the collective velocity of medium. In particular, the medium rest frame is specified as $u_{\text{rest}}^\mu = (1, \mathbf{0})$. The existence of this external vector breaks the Lorentz symmetry, and $\Pi^{\mu\nu}$ now admits two independent tensor structures transverse and longitudinal to u^μ , which will be shown in Eq. (6).

The existence of u^μ splits $P^{\mu\nu}$ into the transverse and longitudinal components such that

$$u_\mu P_T^{\mu\nu} = 0, \quad u_\mu P_L^{\mu\nu} \neq 0, \quad (2)$$

where $P_L^{\mu\nu} + P_T^{\mu\nu} = P^{\mu\nu}$. Both of them remain transverse to the four-momentum and are orthogonal to each other

$$q_\mu P_T^{\mu\nu} = q_\mu P_L^{\mu\nu} = 0, \quad (3)$$

$$P_{T\alpha}^\mu P_L^{\alpha\nu} = 0. \quad (4)$$

In the medium rest frame, the transverse component reads

$$P_T^{00} = P_T^{0i} = P_T^{i0} = 0, \quad P_T^{ij} = q^2 \delta^{ij} - q^i q^j. \quad (5)$$

Note that P_T^{ij} is transverse to spatial momentum q^i , while P_L^{ij} is not. Therefore, they project out polarization modes in the medium rest frame.

By the use of the projection operators, the correlator is decomposed as

$$\Pi^{\mu\nu} = P_T^{\mu\nu} \Pi_T + P_L^{\mu\nu} \Pi_L. \quad (6)$$

Conversely, the scalar amplitudes are extracted as

$$\Pi_L(q^2, v^2) = \frac{1}{v^2} \Pi_{00}(q^2, v^2), \quad (7)$$

$$\Pi_T(q^2, v^2) = -\frac{1}{2} \left[\frac{1}{q^2} \Pi^\mu{}_\mu(q^2, v^2) + \Pi_L(q^2, v^2) \right], \quad (8)$$

where the scalar amplitudes are expressed as functions of q^2 and $v^2 \equiv (u \cdot q)^2 - q^2$. Since the projection operators contain inverse powers of v , these expressions are not evaluated directly at $v = 0$; instead, the projection is carried out at finite v , and then the limit $v \rightarrow 0$ is taken. In this limit, q^μ becomes proportional to u^μ , and the two amplitudes reduce to one, $\Pi_T = \Pi_L$. In the following, we set $u^\mu = u_{\text{rest}}^\mu$.

For each scalar amplitude, a dispersion relation is given as

$$\Pi_X(q^2, v^2) = \int_{-v^2}^{\infty} ds \frac{\rho_X(s, v^2)}{s - q^2}, \quad (X = L, T), \quad (9)$$

where ρ_X is the spectral function, related to the Feynman correlator by

$$\rho_X(q^2, v^2) = \frac{1}{\pi} \tanh\left(\frac{\beta q^0}{2}\right) \text{Im} \Pi_X(q^2, v^2) \quad (q^0 \in \mathbb{R}). \quad (10)$$

Here the positive energy condition $q^0 > 0$ uniquely gives q^0 as a function of q^2 and v^2 .

In Eq. (9), we have suppressed the terms that vanish under the Borel transformation introduced later. More explicitly, the dispersion relation is derived by applying Cauchy's theorem to the correlator, which yields an integral over the spectral function and a surface contribution from the contour at infinity. Both terms are in general divergent, and the divergences are removed by the corresponding subtraction terms. Equation (9) contains only the subtracted integral over the spectral function. The subtracted surface contribution is a polynomial in q^2 with positive powers, which vanishes under the Borel transformation. Note that when Π_X carries a thermal contribution at $q^2 = 0$, an additional term that survives the Borel transformation appears in the dispersion relation; we assume this contribution to be subleading, as discussed in Sec. II E. For details, see Ref. [26, 33].

B. Operator Product Expansion up to Dimension Six

The left-hand side of Eq. (9) is evaluated using the OPE. In the deep Euclidean limit $Q^2 \equiv -q^2 \rightarrow \infty$, the correlator admits a systematic expansion in local operators,

$$\Pi(q^2, v^2) = \sum_n C_n^{\mu_1 \dots \mu_{s_n}}(q^2, v^2) \left\langle \mathcal{O}_{\mu_1 \dots \mu_{s_n}}^{(n)} \right\rangle_T, \quad (11)$$

where the Wilson coefficients C_n encode the short-distance physics and are calculable in perturbation theory, while the local operators $\mathcal{O}^{(n)}$ capture the nonperturbative long-distance effects. The expansion proceeds on an order-by-order basis in operator dimension, with higher-dimensional operators suppressed by inverse powers of Q^2 in the corresponding Wilson coefficients.

We evaluate the OPE of the correlator up to dimension-six operators. The Wilson coefficients used here are derived in Ref. [29]. For convenience, we classify the OPE contributions by operator dimension and spin,

$$\Pi_{\mu\nu}^{\text{OPE}} = \Pi_{\mu\nu}^{\text{scalar}} + \Pi_{\mu\nu}^{4,2} + \Pi_{\mu\nu}^{6,2} + \Pi_{\mu\nu}^{6,4}, \quad (12)$$

where $\Pi_{\mu\nu}^{\text{scalar}}$ collects the scalar operator contributions and $\Pi_{\mu\nu}^{d,s}$ denotes the contribution of operators with dimension d and spin s . The non-scalar condensates vanish in vacuum by the Lorentz symmetry and are therefore purely thermal in origin.

Each part has the Lorentz structure

$$\Pi_{\mu\nu}^{\text{scalar}} = (q_\mu q_\nu - q^2 g_{\mu\nu}) \Pi^{\text{scalar}}, \quad (13)$$

$$\begin{aligned} \Pi_{\mu\nu}^{4,2} = & \frac{1}{Q^2} \left[I_{\mu\nu}^{4,2} + \frac{1}{Q^2} (q^\rho q_\mu I_{\rho\nu}^{4,2} + q^\rho q_\nu I_{\rho\mu}^{4,2}) \right. \\ & + g_{\mu\nu} \frac{q^\rho q^\sigma}{Q^2} J_{\rho\sigma}^{4,2} \\ & \left. + \frac{q_\mu q_\nu q^\rho q^\sigma}{Q^4} (I_{\rho\sigma}^{4,2} + J_{\rho\sigma}^{4,2}) \right], \end{aligned} \quad (14)$$

$$\begin{aligned} \Pi_{\mu\nu}^{6,2} = & \frac{1}{Q^4} \left[I_{\mu\nu}^{6,2} + \frac{1}{Q^2} (q^\rho q_\mu I_{\rho\nu}^{6,2} + q^\rho q_\nu I_{\rho\mu}^{6,2}) \right. \\ & + g_{\mu\nu} \frac{q^\rho q^\sigma}{Q^2} J_{\rho\sigma}^{6,2} \\ & \left. + \frac{q_\mu q_\nu q^\rho q^\sigma}{Q^4} (I_{\rho\sigma}^{6,2} + J_{\rho\sigma}^{6,2}) \right], \end{aligned} \quad (15)$$

$$\begin{aligned} \Pi_{\mu\nu}^{6,4} = & \frac{q^\kappa q^\lambda}{Q^6} \left[I_{\kappa\lambda\mu\nu}^{6,4} + \frac{1}{Q^2} (q^\rho q_\mu I_{\kappa\lambda\rho\nu}^{6,4} + q^\rho q_\nu I_{\kappa\lambda\rho\mu}^{6,4}) \right. \\ & + g_{\mu\nu} \frac{q^\rho q^\sigma}{Q^2} J_{\kappa\lambda\rho\sigma}^{6,4} \\ & \left. + \frac{q_\mu q_\nu q^\rho q^\sigma}{Q^4} (I_{\kappa\lambda\rho\sigma}^{6,4} + J_{\kappa\lambda\rho\sigma}^{6,4}) \right], \end{aligned} \quad (16)$$

where $I^{d,s}, J^{d,s}$ are shorthand tensors defined in Ref. [29], whose explicit expressions in terms of the condensates are given below.

The scalar amplitude Π^{scalar} receives contributions from the unit operator, which gives the purely perturbative part, and from scalar condensates. We expand the perturbative part in powers of α_s and the strange quark mass m_s , retaining terms up to $O(\alpha_s)$ and $O(m_s^4)$,

$$\begin{aligned} \Pi_{\text{pert}}^{\text{scalar}} = & -\frac{1}{4\pi^2} \left(1 + \frac{\alpha_s}{\pi} \right) \ln \frac{Q^2}{\mu^2} \\ & - \frac{3m_s^2}{2\pi^2 Q^2} - \frac{m_s^2 \alpha_s}{\pi^2} \frac{1}{\pi} \frac{1}{Q^2} \left(4 - 3 \ln \frac{Q^2}{\mu^2} \right) \\ & + \frac{m_s^4}{Q^4} \left[\frac{3}{4\pi^2} \left(2 \ln \frac{Q^2}{\mu^2} - 1 \right) \right. \\ & \left. - \frac{1}{6\pi^2} \frac{\alpha_s}{\pi} \left\{ 32 - 24\zeta(3) - 33 \ln \frac{Q^2}{\mu^2} + 18 \left(\ln \frac{Q^2}{\mu^2} \right)^2 \right\} \right]. \end{aligned} \quad (17)$$

For the scalar-condensate contributions, we include terms up to first order in α_s and third order in m_s ; terms of order m_s^4 are absent since they would contribute beyond dimension six,

$$\Pi_{\text{cond}}^{\text{scalar}}(Q^2) = \Pi_{\langle \bar{s}s \rangle}^{\text{scalar}}(Q^2) + \Pi_{\langle G^2 \rangle}^{\text{scalar}}(Q^2) + \Pi_{\text{dim } 6}^{\text{scalar}}(Q^2), \quad (18)$$

where

$$\Pi_{\langle \bar{s}s \rangle}^{\text{scalar}} = \frac{2m_s \langle \bar{s}s \rangle}{Q^4} + \frac{1}{Q^4} \frac{2m_s \alpha_s}{3\pi} \langle \bar{s}s \rangle - \frac{8m_s^3 \langle \bar{s}s \rangle}{3Q^6}, \quad (19)$$

$$\Pi_{\langle G^2 \rangle}^{\text{scalar}} = \frac{1}{Q^4} \frac{7\alpha_s}{288\pi^4} \langle G^2 \rangle + \frac{1}{\pi^2 Q^4} \left(\frac{1}{48} + \frac{1}{36} \frac{m_s^2}{Q^2} \right) \langle G^2 \rangle, \quad (20)$$

$$\begin{aligned} \Pi_{\text{dim } 6}^{\text{scalar}} &= -\frac{4\langle \bar{s}js \rangle}{9Q^6} - \frac{2\langle j_5^2 \rangle}{Q^6} \\ &+ \frac{1}{\pi^2 Q^6} \left(\frac{1}{324} + \frac{1}{54} \ln \frac{Q^2}{\mu^2} \right) \langle j^2 \rangle. \end{aligned} \quad (21)$$

The scalar condensates appearing above are defined as in Ref. [29],

$$\langle G^2 \rangle \equiv \langle g^2 G_{\mu\nu}^a G^{a\mu\nu} \rangle, \quad (22)$$

$$\langle \bar{s}js \rangle \equiv \langle g \bar{s} \gamma^\mu (D^\nu G_{\mu\nu}) s \rangle, \quad (23)$$

$$\langle j_5^2 \rangle \equiv \langle g^2 \bar{s} t^a \gamma_5 \gamma^\mu s \bar{s} t^a \gamma_5 \gamma_\mu s \rangle, \quad (24)$$

$$\langle j^2 \rangle \equiv \langle g^2 (D^\mu G_{\alpha\mu}^a) (D^\nu G^{a\nu}) \rangle. \quad (25)$$

The Wilson coefficients of the non-scalar condensates are retained at leading order in α_s . The quark sector contributes through

$$I_{\mu\nu}^{4,2} = \left(4 - 15 \frac{m_s^2}{Q^2} \right) F_{\mu\nu}, \quad (26)$$

$$J_{\mu\nu}^{4,2} = \left(-4 + 9 \frac{m_s^2}{Q^2} \right) F_{\mu\nu}, \quad (27)$$

$$I_{\mu\nu}^{6,2} = \frac{5}{2} A_{\mu\nu} - \frac{1}{2} B_{\mu\nu} - 13 C_{\mu\nu} + 4 H_{\mu\nu}, \quad (28)$$

$$J_{\mu\nu}^{6,2} = -\frac{3}{2} A_{\mu\nu} + \frac{7}{2} B_{\mu\nu} - 5 C_{\mu\nu} - 4 H_{\mu\nu}, \quad (29)$$

$$I_{\mu\nu\kappa\lambda}^{6,4} = -16i K_{\mu\nu\kappa\lambda}, \quad J_{\mu\nu\kappa\lambda}^{6,4} = 16i K_{\mu\nu\kappa\lambda}, \quad (30)$$

with the non-scalar quark condensates defined as in Ref. [29],

$$A_{\alpha\beta} \equiv \langle \mathcal{ST} g \bar{s} (D^\mu G_{\alpha\mu}) \gamma_\beta s \rangle, \quad (31)$$

$$B_{\alpha\beta} \equiv \langle \mathcal{ST} g \bar{s} \{ i D_\alpha, \tilde{G}_{\beta\mu} \} \gamma_5 \gamma^\mu s \rangle, \quad (32)$$

$$C_{\alpha\beta} \equiv \langle \mathcal{ST} m_s \bar{s} D_\alpha D_\beta s \rangle, \quad (33)$$

$$F_{\alpha\beta} \equiv \langle \mathcal{ST} \bar{s} \gamma_\alpha i D_\beta s \rangle, \quad (34)$$

$$H_{\alpha\beta} \equiv \langle \mathcal{ST} g^2 \bar{s} t^a \gamma_5 \gamma_\alpha s \bar{s} t^a \gamma_5 \gamma_\beta s \rangle, \quad (35)$$

$$K_{\alpha\beta\gamma\delta} \equiv \langle \mathcal{ST} \bar{s} \gamma_\alpha D_\beta D_\gamma D_\delta s \rangle, \quad (36)$$

where $\tilde{G}_{\alpha\beta} = \frac{1}{2} \epsilon_{\alpha\beta\mu\nu} G^{\mu\nu}$ and \mathcal{ST} denotes the symmetric traceless projection. The gluon sector contributes

through

$$I_{\mu\nu}^{4,2} = \left[\frac{1}{8\pi^2} - \frac{47}{48\pi^2} \frac{m_s^2}{Q^2} + \left(-\frac{1}{6\pi^2} + \frac{5}{6\pi^2} \frac{m_s^2}{Q^2} \right) \ln \frac{Q^2}{\mu^2} \right] G_{2\mu\nu}, \quad (37)$$

$$J_{\mu\nu}^{4,2} = \left[-\frac{7}{24\pi^2} + \frac{25}{48\pi^2} \frac{m_s^2}{Q^2} + \left(\frac{1}{6\pi^2} + \frac{1}{6\pi^2} \frac{m_s^2}{Q^2} \right) \ln \frac{Q^2}{\mu^2} \right] G_{2\mu\nu}, \quad (38)$$

$$\begin{aligned} I_{\mu\nu}^{6,2} &= \left(-\frac{1}{60\pi^2} + \frac{1}{96\pi^2} \ln \frac{Q^2}{\mu^2} \right) X_{\mu\nu} \\ &+ \left(-\frac{361}{2880\pi^2} + \frac{3}{32\pi^2} \ln \frac{Q^2}{\mu^2} \right) Y_{\mu\nu} \\ &+ \left(\frac{19}{320\pi^2} + \frac{1}{32\pi^2} \ln \frac{Q^2}{\mu^2} \right) Z_{\mu\nu}, \end{aligned} \quad (39)$$

$$\begin{aligned} J_{\mu\nu}^{6,2} &= \left(-\frac{1}{20\pi^2} - \frac{7}{96\pi^2} \ln \frac{Q^2}{\mu^2} \right) X_{\mu\nu} \\ &+ \left(\frac{149}{960\pi^2} + \frac{1}{96\pi^2} \ln \frac{Q^2}{\mu^2} \right) Y_{\mu\nu} \\ &+ \left(-\frac{239}{960\pi^2} - \frac{7}{32\pi^2} \ln \frac{Q^2}{\mu^2} \right) Z_{\mu\nu}, \end{aligned} \quad (40)$$

$$I_{\mu\nu\kappa\lambda}^{6,4} = \left(-\frac{133}{180\pi^2} + \frac{11}{30\pi^2} \ln \frac{Q^2}{\mu^2} \right) G_{4\mu\nu\kappa\lambda}, \quad (41)$$

$$J_{\mu\nu\kappa\lambda}^{6,4} = \left(\frac{181}{180\pi^2} - \frac{11}{30\pi^2} \ln \frac{Q^2}{\mu^2} \right) G_{4\mu\nu\kappa\lambda}, \quad (42)$$

with the non-scalar gluon condensates defined as in Ref. [29],

$$G_{2\alpha\beta} \equiv \langle \mathcal{ST} g^2 G_{\alpha\mu}^a G_{\beta}^{a\mu} \rangle, \quad (43)$$

$$X_{\alpha\beta} \equiv \langle \mathcal{ST} g^2 G_{\mu\nu}^a D_\beta D_\alpha G^{a\mu\nu} \rangle, \quad (44)$$

$$Y_{\alpha\beta} \equiv \langle \mathcal{ST} g^2 G_{\alpha\mu}^a D^\mu D^\nu G_{\beta\nu}^a \rangle, \quad (45)$$

$$Z_{\alpha\beta} \equiv \langle \mathcal{ST} g^2 G_{\alpha\mu}^a D_\beta D^\nu G^{a\mu\nu} \rangle, \quad (46)$$

$$G_{4\alpha\beta\gamma\delta} \equiv \langle \mathcal{ST} g^2 G_{\alpha\mu}^a D_\delta D_\gamma G_{\beta}^{a\mu} \rangle. \quad (47)$$

The numerical values of all input parameters and condensates are summarized in table I, with further details given in Secs. II C and II D.

C. Scalar Condensates

In this subsection, we provide the numerical inputs for the scalar condensates entering the OPE, given in Sec. II B. Unless otherwise stated, all renormalized quantities are evaluated at $\mu = 1$ GeV in the $\overline{\text{MS}}$ scheme.

1. Quark Scalar Condensate: $\langle \bar{q}q \rangle$ and $\langle \bar{s}s \rangle$

We first specify the vacuum values of quark condensates. We take them from lattice determinations for the light quark [36] and the strange quark [37]. Since these values are given at $\mu = 2$ GeV in the original references,

TABLE I. Input parameters and condensates used in the OPE analysis. All scale-dependent quantities are quoted at $\mu = 1$ GeV, except for $R_g^{(\pi)}$, for which we use the available lattice-QCD value as a reference input.

Quantity	Value	Reference
m_π	139.57061 MeV	[34]
$m_q^{\overline{\text{MS}}}$	4.78 MeV	[34]
$m_s^{\overline{\text{MS}}}$	128 MeV	[34]
$\alpha_s(1 \text{ GeV})$	0.50	[35]
$\langle \bar{q}q \rangle_0$	$-[232(60) \text{ MeV}]^3$	[36]
$\langle \bar{s}s \rangle_0$	$-[196(11) \text{ MeV}]^3$	[37]
$G_0(0)$	$(4\pi^2)(0.012 \pm 0.004) \text{ GeV}^4$	[23, 24]
$T_c^{(l)}, h_l$	166.762 MeV, 0.921635 MeV	[38, 39]
$T_c^{(s)}, h_s$	204.316 MeV, 2.6074 MeV	[38, 39]
h_0, h_1, h_2	0.1396, -0.1800 , 0.0350	[40]
f_0, f_1, f_2	2.76, 6.79, -5.29	[40]
g_1, g_2	-0.47 , 1.04	[40]
$A_2^{\pi(s)}$	0.0257	[41]
$A_2^{\pi(g)}$	0.380	[41]
$A_4^{\pi(s)}$	0.00154	[41]
$A_4^{\pi(g)}$	0.0593	[41]
$R_g^{(\pi)}$	0.388(49)	[42]

we convert them to $\mu = 1$ GeV using renormalization-group-invariant combinations and the running of the quark mass. The numerical values used in the present analysis are listed in table I. Here the light-quark condensate is evaluated in the isospin-symmetric limit, where the up and down quarks are taken to be degenerate with a common mass identified with the average of the physical up and down quark masses.

The temperature dependence of the quark condensates is then captured by the smooth parametrizations fitted to the HotQCD data [38, 39],

$$\frac{\langle \bar{q}q \rangle_T}{\langle \bar{q}q \rangle_0} = \tanh \left[\frac{1}{T} \left(\frac{\langle \bar{q}q \rangle_T}{\langle \bar{q}q \rangle_0} T_c^{(l)} + h_l \right) \right], \quad (48)$$

$$\frac{\langle \bar{s}s \rangle_T}{\langle \bar{s}s \rangle_0} = \tanh \left[\frac{1}{T} \left(\frac{\langle \bar{s}s \rangle_T}{\langle \bar{s}s \rangle_0} T_c^{(s)} + h_s \right) \right], \quad (49)$$

with fit parameters

$$T_c^{(l)} = 166.762 \text{ MeV}, \quad h_l = 0.921635 \text{ MeV}, \quad (50)$$

$$T_c^{(s)} = 204.316 \text{ MeV}, \quad h_s = 2.6074 \text{ MeV}. \quad (51)$$

Since these equations are implicit, the thermal ratios must be obtained by solving them self-consistently at each temperature.

2. Gluon Scalar Condensate: $\langle G^2 \rangle$

For the gluon scalar condensate, we specify the vacuum value and the thermal shift separately. The vacuum value is taken from the standard determination, obtained within the QCD sum rule framework [23, 24],

$$\langle G^2 \rangle_0 = (4\pi^2) (0.012 \pm 0.004) \text{ GeV}^4. \quad (52)$$

The thermal shift $\delta G \equiv \langle G^2 \rangle_T - \langle G^2 \rangle_0$ is evaluated using the trace anomaly relation, which is renormalization-group invariant and gives, at leading order in α_s [43–45],

$$\delta G = -(4\pi^2) \frac{8}{9} \left[\epsilon - 3p - \sum_{f=u,d,s} m_f \delta \langle \bar{f}f \rangle_T \right]. \quad (53)$$

We decompose this into the trace-anomaly and quark-condensate contributions, $\delta G = \delta G^{(l)} + \delta G^{(q)}$, where

$$\delta G^{(l)} = -(4\pi^2) \frac{8}{9} I, \quad I \equiv \epsilon - 3p, \quad (54)$$

$$\delta G^{(q)} = (4\pi^2) \frac{8}{9} \sum_{f=u,d,s} m_f \delta \langle \bar{f}f \rangle_T. \quad (55)$$

For the trace anomaly I , we use the smooth parameterization fitted to the lattice QCD equation of state in Refs. [40, 46],

$$\frac{I(T)}{T^4} = \exp \left(-\frac{h_1}{t} - \frac{h_2}{t^2} \right) \left[h_0 + \frac{f_0 \{ \tanh(f_1 t + f_2) + 1 \}}{1 + g_1 t + g_2 t^2} \right], \quad (56)$$

where $t = T/200$ MeV, with the parameter set of Ref. [40],

$$\begin{aligned} h_0 &= 0.1396, & h_1 &= -0.1800, & h_2 &= 0.0350, \\ f_0 &= 2.76, & f_1 &= 6.79, & f_2 &= -5.29, \\ g_1 &= -0.47, & g_2 &= 1.04. \end{aligned} \quad (57)$$

The quark-condensate contribution $\delta G^{(q)}$ is evaluated using the lattice-based parametrizations of Eqs. (48) and (49), with the quark masses listed in table I [34].

3. Four-Quark Scalar Condensates: $\langle j^2 \rangle$, $\langle j_s^2 \rangle$, $\langle \bar{s}js \rangle$

The dimension-six four-quark condensates are evaluated using the vacuum-saturation approximation ansatz [23, 24, 28], in which a four-quark condensate is approximated as a product of two-quark condensates. This approximation is motivated by large- N_c factorization in vacuum. We apply this approximation also at finite temperature and obtain

$$\langle j^2 \rangle_T = 0, \quad (58)$$

$$\langle j_s^2 \rangle_T = \frac{16}{36} (4\pi\alpha_s) \langle \bar{s}s \rangle_T^2, \quad (59)$$

$$\langle \bar{s}js \rangle_T = -\frac{16}{36} (4\pi\alpha_s) \langle \bar{s}s \rangle_T^2. \quad (60)$$

The first condensate is neglected following Ref. [28], as it is of higher order in α_s than the others.

D. Non-Scalar Condensates

This subsection specifies the numerical inputs for the non-scalar condensates entering the OPE at dimensions

four and six. At finite temperature, the four-velocity u^μ allows spin-two and spin-four operators to acquire non-vanishing expectation values, which vanish in vacuum by Lorentz symmetry. We classify the condensates into three groups: the dimension-four spin-two condensates ($F^{\mu\nu}, G_2^{\mu\nu}$), the dimension-six spin-two condensates ($X_{\alpha\beta}, Y_{\alpha\beta}, Z_{\alpha\beta}, H_{\alpha\beta}$), and the dimension-six spin-four condensates ($K_{\alpha\beta\gamma\delta}, G_{4\alpha\beta\gamma\delta}, A_{\alpha\beta\gamma\delta}, B_{\alpha\beta\gamma\delta}, C_{\alpha\beta\gamma\delta}$). All of these are estimated within the dilute pion-gas approximation. Below the QCD crossover temperature, the thermal medium at vanishing baryon density is dominated by pions, and the dilute pion-gas approximation provides a reasonable description.

1. Dilute Pion-Gas Approximation

At low temperature, the thermal medium is approximated by a dilute gas of pions. Throughout, we use the charged-pion mass listed in table I as a common mass. For a generic operator \mathcal{O} , the thermal expectation value is

$$\begin{aligned} \langle \mathcal{O} \rangle_T &= \langle 0 | \mathcal{O} | 0 \rangle \\ &+ \sum_{A=1}^{d_\pi} \int \frac{d^3k}{2E_{\pi,k}(2\pi)^3} \langle \pi^A(\mathbf{k}) | \mathcal{O} | \pi^A(\mathbf{k}) \rangle n_B(E_{\pi,k}/T), \end{aligned} \quad (61)$$

where $d_\pi = 3$ and $E_{\pi,k} = \sqrt{\mathbf{k}^2 + m_\pi^2}$. The one-pion matrix elements are parametrized in terms of the pion momentum p^μ as

$$\langle \pi^A(p) | \mathcal{O} | \pi^A(p) \rangle = C_{\mathcal{O},0}^\pi, \quad (62)$$

$$\langle \pi^A(p) | \mathcal{O}_{\mu\nu} | \pi^A(p) \rangle = C_{\mathcal{O},2}^\pi \mathcal{ST}(p_\mu p_\nu), \quad (63)$$

$$\langle \pi^A(p) | \mathcal{O}_{\mu_1\mu_2\mu_3\mu_4} | \pi^A(p) \rangle = C_{\mathcal{O},4}^\pi \mathcal{ST}(p_{\mu_1} p_{\mu_2} p_{\mu_3} p_{\mu_4}). \quad (64)$$

Substituting them into Eq. (61) and performing the momentum integral gives

$$\delta \langle \mathcal{O} \rangle_T = d_\pi C_{\mathcal{O},0}^\pi K_0(T; m_\pi), \quad (65)$$

$$\langle \mathcal{O}_{\mu\nu} \rangle_T = d_\pi C_{\mathcal{O},2}^\pi K_2(T; m_\pi) \mathcal{ST}(u_\mu u_\nu), \quad (66)$$

$$\langle \mathcal{O}_{\mu_1\mu_2\mu_3\mu_4} \rangle_T = d_\pi C_{\mathcal{O},4}^\pi K_4(T; m_\pi) \mathcal{ST}(u_{\mu_1} u_{\mu_2} u_{\mu_3} u_{\mu_4}), \quad (67)$$

with

$$K_0(T; m) = \frac{T^2}{24} B_1\left(\frac{m}{T}\right), \quad (68)$$

$$K_2(T; m) = \frac{1}{360} \left[8\pi^2 T^4 B_2\left(\frac{m}{T}\right) - 5m^2 T^2 B_1\left(\frac{m}{T}\right) \right], \quad (69)$$

$$\begin{aligned} K_4(T; m) &= \frac{32\pi^4}{315} T^6 B_3\left(\frac{m}{T}\right) \\ &- \frac{\pi^2}{25} m^2 T^4 B_2\left(\frac{m}{T}\right) + \frac{1}{120} m^4 T^2 B_1\left(\frac{m}{T}\right), \end{aligned} \quad (70)$$

$$B_n(x) = \frac{1}{\zeta(2n)\Gamma(2n)} \int_x^\infty dy y^{2(n-1)} \frac{\sqrt{y^2 - x^2}}{e^y - 1}. \quad (71)$$

In Eqs. (66) and (67), the non-scalar condensates vanish in vacuum by Lorentz invariance, and thus no δ is needed for them. The thermal expectation value of each condensate is then determined by specifying the coefficient $C_{\mathcal{O},n}^\pi$ for the corresponding operator.

2. Dimension-Four Spin-Two Condensates

The dimension-four spin-two condensates are

$$\begin{aligned} F^{\mu\nu} &= \langle \mathcal{ST} \bar{s} \gamma^\mu i D^\nu s \rangle_T \\ &= d_\pi C_{F,2}^\pi K_2(T; m_\pi) \mathcal{ST}(u^\mu u^\nu), \end{aligned} \quad (72)$$

$$\begin{aligned} G_2^{\mu\nu} &= \langle g^2 \mathcal{ST} G_{\mu\nu}^\alpha G^{\alpha\nu} \rangle_T \\ &= d_\pi C_{G,2}^\pi K_2(T; m_\pi) \mathcal{ST}(u^\mu u^\nu). \end{aligned} \quad (73)$$

The coefficients are taken from Ref. [41],

$$C_{F,2}^\pi = A_2^{\pi(s)}|_{\mu=1\text{GeV}} = 0.0257, \quad (74)$$

$$C_{G,2}^\pi = 2(4\pi\alpha_s) \times A_2^{\pi(g)}|_{\mu=1\text{GeV}} = 2(4\pi\alpha_s) \times 0.380, \quad (75)$$

where they are derived from moments of the pion parton distribution functions of Ref. [47].

3. Dimension-Six Spin-Two Condensates

The dimension-six spin-two condensates involve gluon field strengths with two covariant derivatives,

$$\begin{aligned} X_{\alpha\beta} &= \langle g^2 \mathcal{ST} G_{\mu\nu}^\alpha D_\beta D_\alpha G^{\alpha\nu} \rangle \\ &= d_\pi C_{X,2}^\pi K_2(T; m_\pi) \mathcal{ST}(u_\alpha u_\beta), \end{aligned} \quad (76)$$

$$\begin{aligned} Y_{\alpha\beta} &= \langle g^2 \mathcal{ST} G_{\alpha\mu}^\alpha D^\mu D^\nu G_{\beta\nu}^\alpha \rangle \\ &= d_\pi C_{Y,2}^\pi K_2(T; m_\pi) \mathcal{ST}(u_\alpha u_\beta), \end{aligned} \quad (77)$$

$$\begin{aligned} Z_{\alpha\beta} &= \langle g^2 \mathcal{ST} G_{\alpha\mu}^\alpha D_\beta D_\nu G^{\alpha\nu} \rangle \\ &= d_\pi C_{Z,2}^\pi K_2(T; m_\pi) \mathcal{ST}(u_\alpha u_\beta). \end{aligned} \quad (78)$$

To determine the coefficients, we evaluate the one-pion matrix elements using the prescription proposed in Ref. [27]: each covariant derivative acting on a gluon field is replaced by the average gluon four-momentum inside the pion,

$$D_\mu G_{\rho\sigma} \simeq -iR_g^{(\pi)} p_\mu G_{\rho\sigma} , \quad (79)$$

where $R_g^{(\pi)}$ is the gluon momentum fraction in the pion, taken from the lattice-QCD determination at $\mu = 2$ GeV [42],

$$R_g^{(\pi)} = 0.388(49) . \quad (80)$$

Since no determination at $\mu = 1$ GeV is currently available, this value is used as a reference input also for the $\mu = 1$ GeV analysis. Applying the replacement twice gives

$$D_\beta D_\alpha G_{\rho\sigma} \simeq -(R_g^{(\pi)})^2 p_\beta p_\alpha G_{\rho\sigma} , \quad (81)$$

and analogous formulas hold for $D^\mu D^\nu G_{\beta\nu}$ and $D_\beta D_\nu G^{\mu\nu}$. Under this approximation, the coefficients are

$$C_{X,2}^\pi = -(R_g^{(\pi)})^2 C_{G,0}^\pi , \quad (82)$$

$$C_{Y,2}^\pi = (R_g^{(\pi)})^2 \frac{C_{G,0}^\pi + 3C_{G,2}^\pi m_\pi^2}{12} , \quad (83)$$

$$C_{Z,2}^\pi = 3C_{Y,2}^\pi , \quad (84)$$

where $C_{G,0}^\pi$ is the one-pion matrix element of the gluon scalar condensate [30],

$$C_{G,0}^\pi = -\frac{32\pi^2 m_\pi^2}{9} . \quad (85)$$

The remaining dimension-six spin-two condensate $H_{\alpha\beta}$ vanishes under the vacuum-saturation approximation. Under this approximation, the tensor before the symmetric traceless projection takes the form

$$\langle g^2 (\bar{q}t^\alpha \gamma_5 \gamma_\alpha q) (\bar{q}t^\alpha \gamma_5 \gamma_\beta q) \rangle \propto g_{\alpha\beta} \langle \bar{q}q \rangle^2 , \quad (86)$$

which is removed by the \mathcal{ST} projection, giving $H_{\alpha\beta} = 0$.

4. Dimension-Six Spin-Four Condensates

Among the dimension-six spin-four condensates, the condensates $K_{\alpha\beta\gamma\delta}$ and $G_{4\alpha\beta\gamma\delta}$, given by

$$\begin{aligned} K_{\alpha\beta\gamma\delta} &= \langle \mathcal{ST} \bar{q}\gamma_\alpha D_\beta D_\gamma D_\delta q \rangle_T \\ &= d_\pi C_{K,4}^\pi K_4(T; m_\pi) \mathcal{ST}(u^\alpha u^\beta u^\gamma u^\delta) , \end{aligned} \quad (87)$$

$$\begin{aligned} G_{4\alpha\beta\gamma\delta} &= \langle g^2 \mathcal{ST} G_{\alpha\mu}^\alpha D_\delta D_\gamma G_\beta^{\alpha\mu} \rangle_T \\ &= d_\pi C_{G,4}^\pi K_4(T; m_\pi) \mathcal{ST}(u^\alpha u^\beta u^\gamma u^\delta) , \end{aligned} \quad (88)$$

are evaluated using the same procedure as that used for the dimension-four spin-two condensates. This procedure is based on moments of the pion parton distribution

functions of Ref. [47]. The corresponding coefficients are given in Ref. [41] as

$$C_{K,4}^\pi = iA_4^{\pi(s)}|_{\mu=1\text{GeV}} = i0.00154 , \quad (89)$$

$$C_{G,4}^\pi = -2(4\pi\alpha_s) \times A_4^{\pi(g)}|_{\mu=1\text{GeV}} = -2(4\pi\alpha_s) \times 0.0593 . \quad (90)$$

The one-pion matrix elements of the remaining spin-four condensates $A_{\alpha\beta\gamma\delta}$, $B_{\alpha\beta\gamma\delta}$, and $C_{\alpha\beta\gamma\delta}$ are not known, and we neglect these contributions,

$$A_{\alpha\beta\gamma\delta} = B_{\alpha\beta\gamma\delta} = C_{\alpha\beta\gamma\delta} = 0 . \quad (91)$$

This omission introduces a uncertainty in the analysis. However, within the OPE framework, dimension-six operator contributions are expected to be numerically small, and their absence is unlikely to qualitatively affect the results.

E. Phenomenological Modeling of the Spectral Function

This subsection specifies the phenomenological ansatz for the spectral function appearing on the right-hand side of Eq. (9). For each polarization channel $X = L, T$, the spectral function is modeled as a sum of two distinct contributions,

$$\rho_X(s, v^2; T) = \rho_{X,\text{res}}(s, v^2; T) + \rho_{X,\text{high}}(s, v^2; T) , \quad (92)$$

where the first term represents the ϕ meson resonance, while the second term represents the contribution from higher-energy states. In general, thermal contributions such as Landau damping could also enter the spectral function [30]. In the present case, a relevant contribution may arise from the $K\bar{K}$ loop, which lies outside the scope of the pion-gas approximation adopted here; we therefore neglect it. We also note that thermal contributions of this type can carry support at $s = 0$, which would introduce an additional term in the dispersion relation [26, 33].

The ϕ meson resonance is modeled by a delta function,

$$\rho_{X,\text{res}}^\phi(s, v^2; T) = f_{\phi,X}^2(T, v^2) \delta(s - m_{\phi,X}^2(T, v^2)) , \quad (93)$$

where $m_{\phi,X}$ and $f_{\phi,X}$ denote the polarization-dependent mass and decay constant, respectively. This ansatz is motivated by the narrow vacuum width of the ϕ meson ($\Gamma_\phi \simeq 4$ MeV [34]); model analyses suggest that the temperature-induced broadening remains at most ~ 40 MeV at $T = 150$ MeV and vanishing baryon density [12–14, 16–18].

The contribution from higher-energy states is modeled as

$$\rho_{X,\text{high}}(s, v^2; T) = \frac{1}{\pi} \text{Im} \Pi_{\text{pert}}^{\text{scalar}}(s) \theta(s - s_{0,X}) , \quad (94)$$

where $s_{0,X}$ is the threshold marking the onset of continuous higher-energy states. The use of $\frac{1}{\pi} \text{Im} \Pi_{\text{pert}}^{\text{scalar}}$ is motivated by the reliability of the perturbative description

at large s , and is supported empirically by its successful application in QCD sum rule analyses [41]. This perturbative correlator $\Pi_{\text{pert}}^{\text{scalar}}(s)$ is obtained by the analytic continuation from the spacelike expression,

$$\begin{aligned} \Pi_{\text{pert}}^{\text{scalar}}(Q^2) = & -\frac{1 + \alpha_s/\pi}{4\pi^2} \ln \frac{Q^2}{\mu^2} - \frac{3m_s^2}{2\pi^2 Q^2} \\ & - \frac{m_s^2}{\pi^2} \frac{\alpha_s}{\pi} \frac{4 - 3 \ln(Q^2/\mu^2)}{Q^2}, \quad (Q^2 > 0) \end{aligned} \quad (95)$$

via $Q^2 = -s - i0$. The resulting continuum spectral function is

$$\rho_{X,\text{high}}(s, v^2; T) = \left[\frac{1 + \alpha_s(\mu)/\pi}{4\pi^2} + \frac{3m_s^2 \alpha_s(\mu)}{\pi^3 s} \right] \theta(s - s_{0,X}). \quad (96)$$

F. Borel Transformation

The Borel transformation is applied to both sides of the dispersion relation in Eq. (9) to efficiently extract information on the ϕ meson resonance while suppressing the contributions from higher-energy states. The Borel transform of a function $f(Q^2)$ is defined by

$$\mathcal{B}_{M^2}[f] \equiv \lim_{\substack{Q^2, N \rightarrow \infty \\ Q^2/N = M^2}} \frac{(Q^2)^N}{(N-1)!} \left(-\frac{d}{dQ^2} \right)^N f(Q^2). \quad (97)$$

This transformation serves two purposes. First, it eliminates polynomial terms in Q^2 ; as a result, the subtraction terms and the polynomial part of the surface contribution are removed. Second, $1/(s-q^2)$ in the dispersion integral is replaced by $(1/M^2)e^{-s/M^2}$, which exponentially suppresses the high-energy states contribution and enhances the sensitivity to the low-lying ϕ meson resonance [48].

Explicitly, applying the Borel transformation to Eq. (9) gives

$$\mathcal{B}_{M^2}[\Pi_X(q^2, v^2)] = \Pi_X^{\text{res}}(M^2, v^2) + \Pi_X^{\text{high}}(M^2, v^2). \quad (98)$$

where the resonance term is

$$\begin{aligned} \Pi_X^{\text{res}}(M^2, v^2) &= \frac{1}{M^2} \int_{-v^2}^{\infty} ds \rho_{X,\text{res}} e^{-s/M^2} \\ &= \frac{f_{\phi,X}^2(T, v^2)}{M^2} \exp \left[-\frac{m_{\phi,X}^2(T, v^2)}{M^2} \right], \end{aligned} \quad (99)$$

while high-energy states part is

$$\begin{aligned} \Pi_X^{\text{high}}(M^2, v^2) &= \frac{1}{M^2} \int_{-v^2}^{\infty} ds \rho_{X,\text{cont}} e^{-s/M^2} \\ &= \frac{1 + \alpha_s(\mu)/\pi}{4\pi^2} e^{-s_{0,X}(T, v)/M^2} \\ &+ \frac{3m_s^2 \alpha_s(\mu)}{\pi^3 M^2} E_1 \left(\frac{s_{0,X}(T, v)}{M^2} \right), \end{aligned} \quad (100)$$

with

$$E_1(x) \equiv \int_x^{\infty} dt \frac{e^{-t}}{t} = \Gamma(0, x). \quad (101)$$

When $s_{0,X} \gg m_{\phi,X}^2$, the two contributions are well separated, and the sum rule provides a reliable constraint on parameters in the vector-meson spectral function. Explicit forms of the Borel-transformed OPE side of Eq. (98) is quite long, and is given in Appendix A (which is the same expression as shown in Ref. [28]).

III. NUMERICAL RESULTS

We present the numerical results of the ϕ meson properties at finite temperature. We first describe the zero-momentum results, where the longitudinal and transverse channels are degenerate. We then study the finite-momentum dependence and analyze the longitudinal-transverse splitting for different temperatures. Finally, we examine the origin of the splitting by selectively removing thermal contributions in the operator product expansion.

A. Numerical analysis method

Before presenting the numerical results, we summarize the procedure used to extract the ϕ meson mass and decay constant from the Borel sum rule. The analysis is based on the rearranged form of Eq. (98),

$$\mathcal{A}_X(M^2, v^2; s_0) = \Pi_X^{\text{res}}(M^2, v^2), \quad (102)$$

with

$$\mathcal{A}_X(M^2, v^2; s_0) \equiv \mathcal{B}_{M^2}[\Pi_X(q^2, v^2)] - \Pi_X^{\text{high}}(M^2, v^2). \quad (103)$$

For each temperature T , momentum v , and channel $X = L, T$, we independently determine the optimal continuum threshold $s_{0,X}^*(T, v)$ and extract the corresponding ϕ meson mass and decay constant.

As the first step, we determine the so-called Borel window

$$M_{\text{min},X}(v^2, T) \leq M \leq M_{\text{max},X}(v^2, T; s_0), \quad (104)$$

for given s_0 , T , and v . The window, within which the analysis is considered reliable, is defined by two conditions. The lower boundary $M_{\text{min},X}$ is set by the OPE convergence condition,

$$C_X(M^2, v^2) = \left| \frac{\mathcal{B}_{M^2}[\Pi_X^{(d=6)}(q^2, v^2)]}{\mathcal{B}_{M^2}[\Pi_X(q^2, v^2)]} \right| \leq 0.1, \quad (105)$$

where $\Pi_X^{(d=6)}$ denotes the dimension-six contribution to $\Pi_X(q^2, v^2)$. The upper boundary $M_{\max, X}$ is set by the pole-dominance condition,

$$P_X(M^2, v^2; s_0) = \left| \frac{A_X(M^2, v^2; s_0)}{\mathcal{B}_{M^2}[\Pi_X(q^2, v^2)]} \right| \geq 0.5. \quad (106)$$

If a Borel window satisfying both the OPE-convergence and pole-dominance conditions cannot be defined, the corresponding trial value of s_0 is discarded.

Within the Borel window, the ϕ meson mass and its decay constant for generic M^2 are extracted as

$$m_{\phi, X}^2(M^2, v^2; s_0) = M^2 - \frac{dA_X(M^2, v^2; s_0)/d(M^{-2})}{A_X(M^2, v^2; s_0)}, \quad (107)$$

$$f_{\phi, X}^2(M^2, v^2; s_{0, X}) = M^2 A_X(M^2, v^2; s_{0, X}) \times \exp\left[\frac{m_{\phi, X}^2(M^2, v^2; s_{0, X})}{M^2}\right]. \quad (108)$$

The Borel-window averages are then

$$\bar{m}_{\phi, X}(v^2; s_0) = \frac{\int_{M_{\min, X}}^{M_{\max, X}} dM m_{\phi, X}(M^2, v^2; s_0)}{M_{\max, X} - M_{\min, X}}, \quad (109)$$

$$\bar{f}_{\phi, X}(v^2; s_0) = \frac{\int_{M_{\min, X}}^{M_{\max, X}} dM f_{\phi, X}(M^2, v^2; s_0)}{M_{\max, X} - M_{\min, X}}, \quad (110)$$

where the arguments of $M_{\min, X}$ and $M_{\max, X}$ are omitted for notational simplicity. Stability of the extracted mass with respect to the Borel mass is estimated with a variance

$$\chi_{m, X}^2(v^2; s_0) = \frac{\int_{M_{\min, X}}^{M_{\max, X}} dM [m_{\phi, X}(M^2, v^2; s_0) - \bar{m}_{\phi, X}(v^2; s_0)]^2}{M_{\max, X} - M_{\min, X}}. \quad (111)$$

This quantity serves as a stability measure of the Borel-mass dependence and is not a statistical chi-square. The continuum threshold is determined as the value of s_0 that minimizes $\chi_{m, X}^2$, i.e.,

$$s_{0, X}^*(T, v^2) = \arg \min_{s_0} \chi_{m, X}^2(T, v^2; s_0). \quad (112)$$

The ϕ meson mass and its decay constant are then determined as

$$m_{\phi, X}(T, v^2) = \bar{m}_{\phi, X}(T, v^2; s_{0, X}^*(T, v^2)), \quad (113)$$

$$f_{\phi, X}(T, v^2) = \bar{f}_{\phi, X}(T, v^2; s_{0, X}^*(T, v^2)). \quad (114)$$

B. Temperature dependence at zero momentum

We first consider the zero-momentum case, $v = |\mathbf{q}| = 0$. In this limit, the longitudinal and transverse channels are degenerate, and the analysis reduces to that for

a single scalar amplitude. Figure 1 shows the stability measure $\chi_m^2 = \chi_{m, X}^2(v^2 = 0; s_0)$ as a function of the continuum threshold s_0 at representative temperatures $T = 0.0, 0.05, 0.1, 0.15$ GeV. The minimum of χ_m^2 determines the optimal threshold s_0^* used in the subsequent analysis. In practice, the scan over s_0 is performed with a grid spacing of $\Delta s_{0, X} = 0.001$ GeV², which is sufficiently small compared with the overall scale of variation of χ_m^2 . In the figure, χ_m^2 shows little variation in the range $T = 0.0$ – 0.05 GeV, while for $T = 0.05$ – 0.15 GeV the position of the minimum is seen to shift progressively toward smaller values of s_0 .

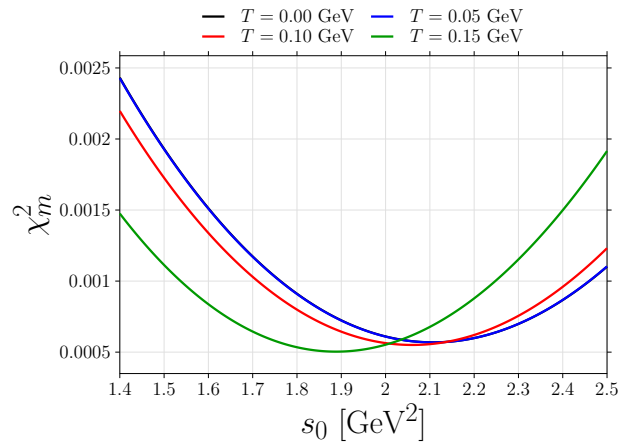


FIG. 1. Stability measure χ_m^2 as a function of the continuum threshold s_0 at zero momentum for representative temperatures $T = 0.0, 0.05, 0.1, 0.15$ GeV. The minimum of each curve determines the optimal continuum threshold s_0^* .

Using the optimized value of s_0 , we next study the temperature dependence at zero momentum. Figure 2 shows the temperature dependence of m_ϕ , f_ϕ , and s_0^* in the range $0 \text{ GeV} \leq T \leq 0.15 \text{ GeV}$. All three quantities remain nearly constant for $T \lesssim 0.06 \text{ GeV}$ and then decrease at higher temperatures. All the three quantities exhibit a monotonic dependence on temperature for $T \gtrsim 0.06 \text{ GeV}$. This correlated behavior was also reported in the QCD sum rule analysis of the ϕ meson in nuclear matter [28]

C. Momentum dependence and transverse and longitudinal splitting

We next turn to the finite-momentum regime $v \neq 0$, where the longitudinal and transverse channels of the current-current correlator, defined with respect to the medium rest frame, become distinct. Consequently, the properties of the ϕ meson should be determined separately for the two channels. Figure 3 shows the momentum dependence of the ϕ -meson mass for the transverse and longitudinal channels at $T = 0.05, 0.10$, and 0.15 GeV . At small momentum, the two channels are

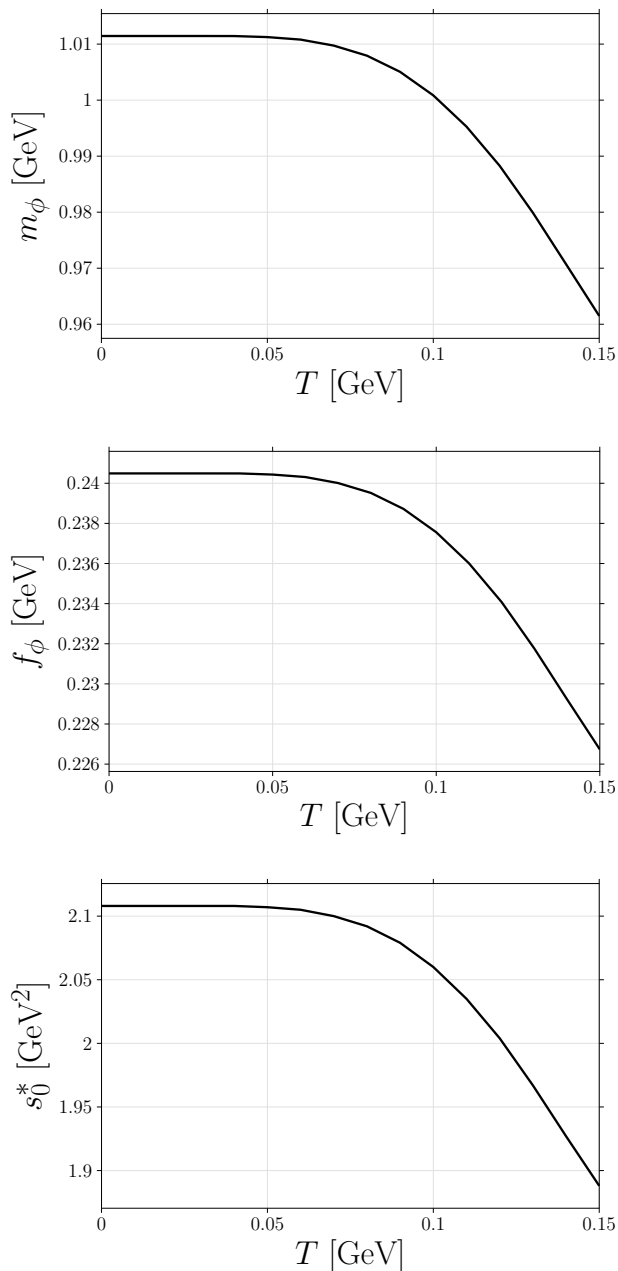


FIG. 2. Temperature dependence of the pole parameters at zero momentum. The panels show the ϕ meson mass m_ϕ , the residue f_ϕ , and the continuum threshold s_0 . The temperature range is $0 \leq T \leq 0.15$ GeV.

nearly degenerate, confirming the expected degeneracy in the low-momentum limit. As v increases, both masses rise and a clear splitting develops between them, with the transverse mass exceeding the longitudinal mass. The magnitude of this splitting grows with temperature.

The finite-temperature mass splitting obtained here for $T = 0.1$ GeV is much smaller than the nuclear matter counterpart reported in the QCD sum rule analysis of Ref. [28] and the recent quark-meson coupling model

analysis of Ref. [20], where the longitudinal-transverse splitting reaches the order of tens of MeV. However, at $T = 0.15$ GeV, the splitting is of the same order of magnitude as that obtained in the above works for dense matter at normal nuclear matter density. This tendency is consistent with theoretical calculations based on hadronic models that systematically estimate both nuclear matter and finite-temperature effects within a unified framework [16–18].

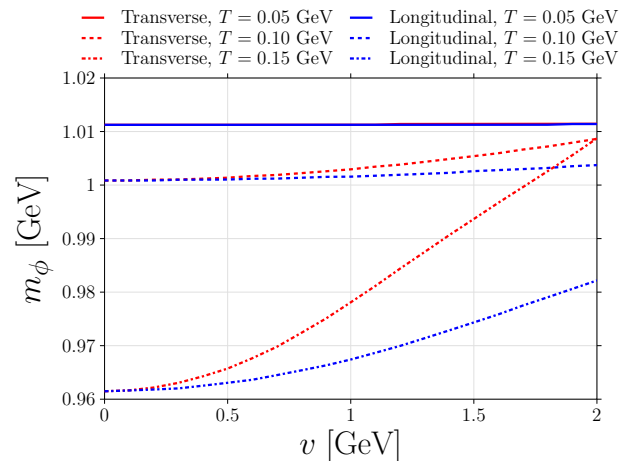


FIG. 3. Momentum dependence of the ϕ meson mass at fixed temperatures. Red and blue lines show the transverse and longitudinal channels, respectively. Solid, dashed, and dash-dotted lines correspond to $T = 0.05$, 0.10 , and 0.15 GeV, respectively.

D. Origin of the transverse and longitudinal splitting

Finally, we investigate which thermal contributions are responsible for the transverse and longitudinal splitting. To this end, we compare the full result with those from modified analyses in which selected leading tensor condensate terms in the OPE are switched off. The leading tensor terms appear with the dimension-four quark condensate F with one derivative and gluon condensate G_2 , evaluated in Sec. II D 2. Here, we suppress the Lorentz indices on those condensates for notational simplicity.

Figure 4 compares the transverse-longitudinal mass splitting, $m_{\phi,T} - m_{\phi,L}$, at $T = 0.10$ GeV, among the full result, the result obtained by switching off the F condensate alone, and the result obtained by switching off both the F and G_2 condensates. The full result shows a clear momentum-dependent splitting. When the F condensate is switched off, the splitting is clearly reduced, and it is further suppressed when both the F and G_2 condensates are switched off. This comparison indicates that the transverse-longitudinal mass splitting is mainly driven by the dimension-four condensates.

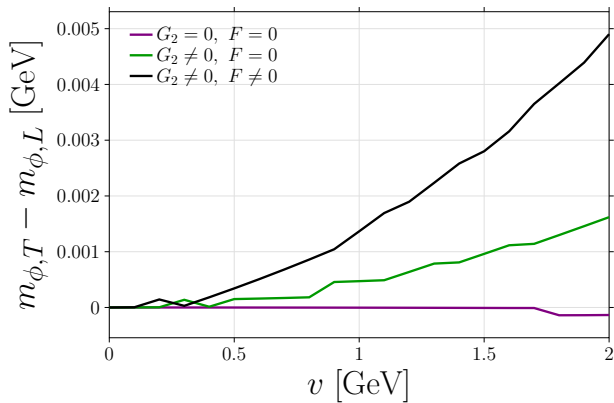


FIG. 4. Comparison of the transverse-longitudinal mass splitting of the ϕ meson with and without the dimension-four condensate terms F and G_2 at $T = 0.10$ GeV. The black, green, and purple lines show the results obtained by including both condensates, switching off the F condensate alone, and switching off both the F and G_2 condensates, respectively.

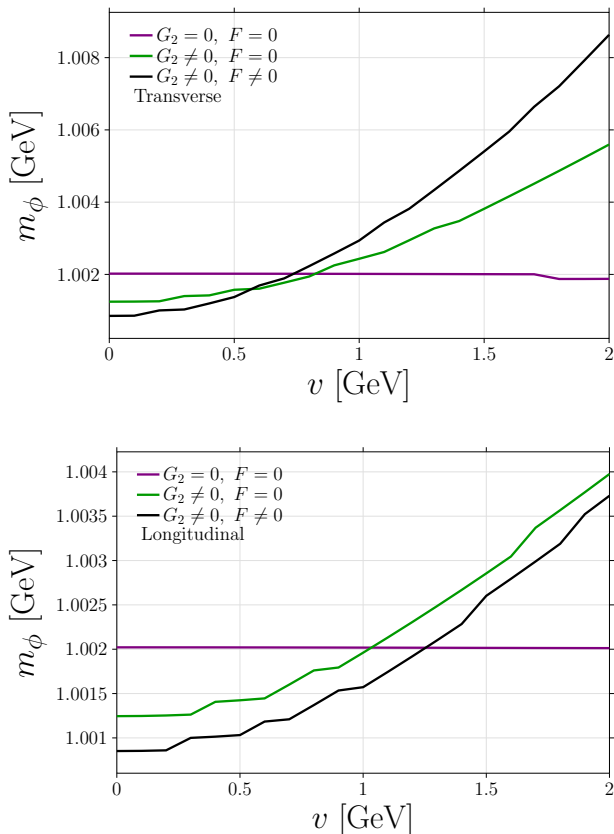


FIG. 5. Same as Fig. 4, but the upper and lower panels show the transverse and longitudinal channels separately at $T = 0.10$ GeV, respectively.

Figure 5 shows the momentum dependence of the ϕ meson mass at $T = 0.10$ GeV in the transverse and longitudinal channels. In each plot, we compare the full result with those obtained by selectively switching off the dimension-four thermal condensates, F and G_2 . In the transverse channel, as shown in the upper panel, both condensates contribute comparably in magnitude to the upward mass shift at large momentum. In the longitudinal channel, as shown in the lower panel, switching off the F condensate has a relatively minor effect on the result. The residual major momentum dependence stems from the G_2 condensate. These comparisons indicate that the G_2 condensate gives the dominant contribution to the mass shift in the longitudinal channel, while the F condensate also gives a comparable contribution in the transverse channel.

IV. SUMMARY

We have studied the ϕ meson at finite temperature and finite momentum using QCD sum rules. The strange vector current correlator has been decomposed into the transverse and longitudinal channels with respect to the medium flow vector. The operator product expansion has been evaluated up to dimension six, including scalar condensates and non-scalar condensates. The non-scalar condensates, which have purely thermal origin, have been estimated in the dilute pion-gas approximation. At zero momentum, the transverse and longitudinal channels are degenerate. In this limit, we have found that the optimized continuum threshold, the ϕ meson mass, and the decay constant remain nearly constant for $T \lesssim 0.06$ GeV and decrease for $0.06 \text{ GeV} \lesssim T \lesssim 0.15$ GeV.

At finite momentum, the transverse and longitudinal channels split. We have found that both masses increase with momentum, with the transverse mass exceeding the longitudinal mass. Also, we have found that the size of this splitting grows with temperature. We have further investigated the origin of the finite-momentum splitting by selectively removing dimension-four thermal condensate contributions. The comparison has shown that the G_2 condensate gives the dominant contribution to the mass shifts, especially in the longitudinal channel, while both the G_2 and F condensates give visible contributions to the transverse-longitudinal difference.

As a future direction, it is important to connect the finite-temperature modifications of the transverse and longitudinal spectral functions obtained in this work to experimentally accessible signals. This requires a more explicit treatment of the dilepton and $K\bar{K}$ decay channels, which would allow one to estimate how the finite-temperature transverse-longitudinal splitting appears in measured spectra. It is also interesting to examine effects from thermal kaon excitations, including possible Landau-damping contributions. Although this effect is naively suppressed in the low-temperature range considered here due to a suppressed thermal distribution, it

could be sizable because of a direct coupling to the ϕ meson through strange hadronic channels.

where $L_Q = \ln(Q^2/\mu^2)$ and $\psi(n)$ is the digamma function.

ACKNOWLEDGMENTS

This work is supported by the National Natural Science Foundation of China (NSFC) under grant numbers W2433010 and W2532002 and by JSPS KAKENHI under grant numbers JP25H00400, JP26K07113, and 23K22487.

Appendix A: Borel-transformed OPE expressions

In this appendix, we summarize the explicit Borel-transformed OPE expressions used in the numerical analysis. For convenience, we define

$$\mathcal{I}_n(M^2) \equiv \mathcal{B}_{M^2} \left[\frac{1}{(Q^2)^n} \right] = \frac{1}{(n-1)!} \frac{1}{(M^2)^n}, \quad (\text{A1})$$

$$\mathcal{L}_n(M^2) \equiv \mathcal{B}_{M^2} \left[\frac{L_Q}{(Q^2)^n} \right] = \left[\ln \frac{M^2}{\mu^2} + \psi(n) \right] \mathcal{I}_n(M^2), \quad (\text{A2})$$

$$\begin{aligned} \mathcal{K}_n(M^2) &\equiv \mathcal{B}_{M^2} \left[\frac{L_Q^2}{(Q^2)^n} \right] \\ &= \left[\left(\ln \frac{M^2}{\mu^2} + \psi(n) \right)^2 - \dot{\psi}(n) \right] \mathcal{I}_n(M^2), \quad (\text{A3}) \end{aligned}$$

The longitudinal OPE after the Borel transformation is

$$\begin{aligned} \mathcal{B}_{M^2} [\Pi_L(q^2, v^2)] &= \frac{1 + \alpha_s/\pi}{4\pi^2} - \frac{3m_s^2}{2\pi^2} \mathcal{I}_1 - \frac{m_s^2 \alpha_s}{\pi^2 \pi} (4\mathcal{I}_1 - 3\mathcal{L}_1) \\ &+ 2m_s \langle \bar{s}s \rangle \mathcal{I}_2 + \frac{2m_s \alpha_s}{3\pi} \langle \bar{s}s \rangle \mathcal{I}_2 - \frac{8m_s^3 \langle \bar{s}s \rangle}{3} \mathcal{I}_3 - \frac{4\langle \bar{s}j s \rangle}{9} \mathcal{I}_3 - 2\langle j_5^2 \rangle \mathcal{I}_3 \\ &+ \frac{\langle G^2 \rangle}{\pi^2} \left(\frac{1}{48} \mathcal{I}_2 + \frac{m_s^2}{36} \mathcal{I}_3 \right) + \frac{7\alpha_s}{288\pi^4} \langle G^2 \rangle \mathcal{I}_2 + \frac{3m_s^4}{4\pi^2} (2\mathcal{L}_2 - \mathcal{I}_2) \\ &- \frac{m_s^4 \alpha_s}{6\pi^2 \pi} \left(32\mathcal{I}_2 - 24\zeta(3)\mathcal{I}_2 - 33\mathcal{L}_2 + 18\mathcal{K}_2 \right) \\ &+ (2\mathcal{I}_2 - 3m_s^2 \mathcal{I}_3 - 6m_s^2 v^2 \mathcal{I}_4) \widehat{F} \\ &+ \frac{\widehat{G}_2}{48\pi^2} \left[-4\mathcal{L}_2 - 16m_s^2 \mathcal{L}_3 + 48m_s^2 v^2 \mathcal{L}_4 + 9\mathcal{I}_2 - 11m_s^2 \mathcal{I}_3 - 8v^2 \mathcal{I}_3 - 22m_s^2 v^2 \mathcal{I}_4 \right] \\ &+ \frac{\widehat{X}}{480\pi^2} \left[25\mathcal{L}_3 - 30v^2 \mathcal{L}_4 + 20\mathcal{I}_3 - 32v^2 \mathcal{I}_4 \right] + \frac{\widehat{Y}}{2880\pi^2} \left[-90\mathcal{L}_3 + 300v^2 \mathcal{L}_4 - 245\mathcal{I}_3 + 86v^2 \mathcal{I}_4 \right] \\ &+ \frac{\widehat{Z}}{960\pi^2} \left[150\mathcal{L}_3 - 180v^2 \mathcal{L}_4 + 165\mathcal{I}_3 - 182v^2 \mathcal{I}_4 \right] + \frac{2i}{3} (5\mathcal{I}_3 - 6v^2 \mathcal{I}_4) \widehat{K} \\ &+ \frac{\widehat{G}_4}{4320\pi^2} \left[-330\mathcal{L}_3 + 396v^2 \mathcal{L}_4 + 1025\mathcal{I}_3 - 2238v^2 \mathcal{I}_4 + 1152v^4 \mathcal{I}_5 \right]. \quad (\text{A4}) \end{aligned}$$

The transverse OPE after the Borel transformation is

$$\begin{aligned}
\mathcal{B}_{M^2}[\Pi_T(q^2, v^2)] &= \frac{1 + \alpha_s/\pi}{4\pi^2} - \frac{3m_s^2}{2\pi^2} \mathcal{I}_1 - \frac{m_s^2 \alpha_s}{\pi^2 \pi} (4\mathcal{I}_1 - 3\mathcal{L}_1) \\
&+ 2m_s \langle \bar{s}s \rangle \mathcal{I}_2 + \frac{2m_s \alpha_s}{3\pi} \langle \bar{s}s \rangle \mathcal{I}_2 - \frac{8m_s^3 \langle \bar{s}s \rangle}{3} \mathcal{I}_3 - \frac{4 \langle \bar{s}j s \rangle}{9} \mathcal{I}_3 - 2 \langle j_5^2 \rangle \mathcal{I}_3 \\
&+ \frac{\langle G^2 \rangle}{\pi^2} \left(\frac{1}{48} \mathcal{I}_2 + \frac{m_s^2}{36} \mathcal{I}_3 \right) + \frac{7\alpha_s}{288\pi^4} \langle G^2 \rangle \mathcal{I}_2 + \frac{3m_s^4}{4\pi^2} (2\mathcal{L}_2 - \mathcal{I}_2) \\
&- \frac{m_s^4 \alpha_s}{6\pi^2 \pi} \left(32\mathcal{I}_2 - 24\zeta(3)\mathcal{I}_2 - 33\mathcal{L}_2 + 18\mathcal{K}_2 \right) \\
&+ (2\mathcal{I}_2 - 4v^2\mathcal{I}_3 - 3m_s^2\mathcal{I}_3 + 9m_s^2v^2\mathcal{I}_4) \widehat{F} \\
&+ \frac{\widehat{G}_2}{48\pi^2} \left[-4\mathcal{L}_2 - 16m_s^2\mathcal{L}_3 + 8v^2\mathcal{L}_3 + 8m_s^2v^2\mathcal{L}_4 + 9\mathcal{I}_2 - 11m_s^2\mathcal{I}_3 - 14v^2\mathcal{I}_3 + 33m_s^2v^2\mathcal{I}_4 \right] \\
&+ \frac{\widehat{X}}{480\pi^2} \left[25\mathcal{L}_3 - 35v^2\mathcal{L}_4 + 20\mathcal{I}_3 - 24v^2\mathcal{I}_4 \right] + \frac{\widehat{Y}}{2880\pi^2} \left[-90\mathcal{L}_3 + 30v^2\mathcal{L}_4 - 245\mathcal{I}_3 + 447v^2\mathcal{I}_4 \right] \\
&+ \frac{\widehat{Z}}{960\pi^2} \left[150\mathcal{L}_3 - 210v^2\mathcal{L}_4 + 165\mathcal{I}_3 - 239v^2\mathcal{I}_4 \right] + \frac{2i}{3} (5\mathcal{I}_3 - 27v^2\mathcal{I}_4 + 24v^4\mathcal{I}_5) \widehat{K} \\
&+ \frac{\widehat{G}_4}{4320\pi^2} \left[-330\mathcal{L}_3 + 1782v^2\mathcal{L}_4 - 1584v^4\mathcal{L}_5 + 1025\mathcal{I}_3 - 5031v^2\mathcal{I}_4 + 4344v^4\mathcal{I}_5 \right]. \tag{A5}
\end{aligned}$$

For reference, we write down the explicit form of \mathcal{I}_n ($n = 1, 2, \dots, 5$),

$$\mathcal{I}_1(M^2) = \frac{1}{M^2}, \tag{A6}$$

$$\mathcal{I}_2(M^2) = \frac{1}{(M^2)^2}, \tag{A7}$$

$$\mathcal{I}_3(M^2) = \frac{1}{2(M^2)^3}, \tag{A8}$$

$$\mathcal{I}_4(M^2) = \frac{1}{6(M^2)^4}, \tag{A9}$$

$$\mathcal{I}_5(M^2) = \frac{1}{24(M^2)^5}. \tag{A10}$$

The logarithmic functions \mathcal{L}_n needed above are

$$\mathcal{L}_1(M^2) = \left(\ln \frac{M^2}{\mu^2} - \gamma_E \right) \frac{1}{M^2}, \tag{A11}$$

$$\mathcal{L}_2(M^2) = \left(\ln \frac{M^2}{\mu^2} + 1 - \gamma_E \right) \frac{1}{(M^2)^2}, \tag{A12}$$

$$\mathcal{L}_3(M^2) = \left(\ln \frac{M^2}{\mu^2} + \frac{3}{2} - \gamma_E \right) \frac{1}{2(M^2)^3}, \tag{A13}$$

$$\mathcal{L}_4(M^2) = \left(\ln \frac{M^2}{\mu^2} + \frac{11}{6} - \gamma_E \right) \frac{1}{6(M^2)^4}, \tag{A14}$$

$$\mathcal{L}_5(M^2) = \left(\ln \frac{M^2}{\mu^2} + \frac{25}{12} - \gamma_E \right) \frac{1}{24(M^2)^5}. \tag{A15}$$

We also use

$$\mathcal{K}_2(M^2) = \left[\left(\ln \frac{M^2}{\mu^2} + 1 - \gamma_E \right)^2 - \left(\frac{\pi^2}{6} - 1 \right) \right] \frac{1}{(M^2)^2}. \tag{A16}$$

[1] J. J. Dudek, R. G. Edwards, P. Guo, and C. E. Thomas (Hadron Spectrum), Toward the excited isoscalar meson spectrum from lattice QCD, Phys. Rev. D **88**, 094505

(2013), arXiv:1309.2608 [hep-lat].

[2] T. Ishikawa *et al.*, phi photo-production from Li, C, Al, and Cu nuclei at E(gamma) = 1.5-GeV to 2.4-GeV, Phys.

- Let. B **608**, 215 (2005), arXiv:nucl-ex/0411016.
- [3] R. Muto *et al.* (KEK-PS-E325), Evidence for in-medium modification of the phi meson at normal nuclear density, Phys. Rev. Lett. **98**, 042501 (2007), arXiv:nucl-ex/0511019.
- [4] F. Sakuma *et al.* (E325), Study of nuclear matter modification of decay widths in $\phi \rightarrow e^+ e^-$ and $\phi \rightarrow K^+ K^-$ channels, Phys. Rev. Lett. **98**, 152302 (2007), arXiv:nucl-ex/0606029.
- [5] M. H. Wood *et al.* (CLAS), Absorption of the ω and ϕ Mesons in Nuclei, Phys. Rev. Lett. **105**, 112301 (2010), arXiv:1006.3361 [nucl-ex].
- [6] A. Polyanskiy *et al.*, Measurement of the in-medium phi-meson width in proton-nucleus collisions, Phys. Lett. B **695**, 74 (2011), arXiv:1008.0232 [nucl-ex].
- [7] M. Hartmann *et al.*, Momentum dependence of the phi-meson nuclear transparency, Phys. Rev. C **85**, 035206 (2012), arXiv:1201.3517 [nucl-ex].
- [8] J. Adamczewski-Musch *et al.* (HADES), Strong absorption of hadrons with hidden and open strangeness in nuclear matter, Phys. Rev. Lett. **123**, 022002 (2019), arXiv:1812.03728 [nucl-ex].
- [9] M. Ichikawa *et al.* (KEK-PS E325), Analysis of Spectral Modification of φ Mesons at Finite Density Using a Transport Approach in 12 GeV pA Reactions, PTEP **2025**, 093D01 (2025), arXiv:2507.00420 [nucl-ex].
- [10] M. Asakawa and C. M. Ko, Phi meson mass in hot and dense matter, Nucl. Phys. A **572**, 732 (1994).
- [11] S. Zschocke, O. P. Pavlenko, and B. Kampfer, Evaluation of QCD sum rules for light vector mesons at finite density and temperature, Eur. Phys. J. A **15**, 529 (2002), arXiv:nucl-th/0205057.
- [12] D. Lissauer and E. V. Shuryak, K meson modification in hot hadronic matter may be detected via Phi meson decays, Phys. Lett. B **253**, 15 (1991).
- [13] C. M. Ko and D. Seibert, What can we learn from a second phi meson peak in ultrarelativistic nuclear collisions?, Phys. Rev. C **49**, 2198 (1994), arXiv:nucl-th/9312010.
- [14] K. L. Haglin and C. Gale, Properties of the phi meson at finite temperature, Nucl. Phys. B **421**, 613 (1994), arXiv:nucl-th/9401003.
- [15] C. Song, Effective mass of phi mesons at finite temperature, Phys. Lett. B **388**, 141 (1996), arXiv:hep-ph/9603259.
- [16] G. Vujanovic, J. Ruppert, and C. Gale, The phi meson at high temperatures and densities, Phys. Rev. C **80**, 044907 (2009), arXiv:0907.5385 [nucl-th].
- [17] R. Kumar and A. Kumar, ϕ meson mass and decay width in strange hadronic matter, Phys. Rev. C **102**, 045206 (2020), arXiv:2005.05133 [hep-ph].
- [18] M. Kaur and A. Kumar, ϕ meson properties in dense resonance matter at finite temperature, Phys. Rev. D **112**, 014030 (2025), arXiv:2505.07065 [hep-ph].
- [19] I. W. Park, H. Sako, K. Aoki, P. Gubler, and S. H. Lee, Disentangling longitudinal and transverse modes of the ϕ meson through dilepton and kaon decays, Phys. Rev. D **107**, 074033 (2023), arXiv:2211.16949 [hep-ph].
- [20] A. J. Arifi, P. Gubler, and K. Tsushima, Polarization-dependent mass modifications of ϕ meson with finite momentum in nuclear matter (2026), arXiv:2603.15971 [hep-ph].
- [21] S. Acharya *et al.* (ALICE), Evidence of Spin-Orbital Angular Momentum Interactions in Relativistic Heavy-Ion Collisions, Phys. Rev. Lett. **125**, 012301 (2020), arXiv:1910.14408 [nucl-ex].
- [22] M. S. Abdallah *et al.* (STAR), Pattern of global spin alignment of ϕ and K^{*0} mesons in heavy-ion collisions, Nature **614**, 244 (2023), arXiv:2204.02302 [hep-ph].
- [23] M. A. Shifman, A. I. Vainshtein, and V. I. Zakharov, QCD and Resonance Physics. Theoretical Foundations, Nucl. Phys. B **147**, 385 (1979).
- [24] M. A. Shifman, A. I. Vainshtein, and V. I. Zakharov, QCD and Resonance Physics: Applications, Nucl. Phys. B **147**, 448 (1979).
- [25] T. Hatsuda and S. H. Lee, QCD sum rules for vector mesons in the nuclear medium, Phys. Rev. C **46**, R34 (1992).
- [26] F. Klingl, N. Kaiser, and W. Weise, Current correlation functions, QCD sum rules and vector mesons in baryonic matter, Nucl. Phys. A **624**, 527 (1997), arXiv:hep-ph/9704398.
- [27] S. H. Lee, Vector mesons in-medium with finite three momentum, Phys. Rev. C **57**, 927 (1998), [Erratum: Phys.Rev.C 58, 3771 (1998)], arXiv:nucl-th/9705048.
- [28] H. Kim and P. Gubler, The ϕ meson with finite momentum in a dense medium, Phys. Lett. B **805**, 135412 (2020), arXiv:1911.08737 [hep-ph].
- [29] H. Kim, P. Gubler, and S. H. Lee, Light vector correlator in medium: Wilson coefficients up to dimension 6 operators, Phys. Lett. B **772**, 194 (2017), [Erratum: Phys.Lett.B 779, 498–498 (2018)], arXiv:1703.04848 [hep-ph].
- [30] T. Hatsuda, Y. Koike, and S.-H. Lee, Finite temperature QCD sum rules reexamined: rho, omega and A1 mesons, Nucl. Phys. B **394**, 221 (1993).
- [31] P. Gubler and M. Oka, A Bayesian approach to QCD sum rules, Prog. Theor. Phys. **124**, 995 (2010), arXiv:1005.2459 [hep-ph].
- [32] H.-n. Li and H. Umeeda, QCD sum rules with spectral densities solved in inverse problems, Phys. Rev. D **102**, 114014 (2020), arXiv:2006.16593 [hep-ph].
- [33] S. Leupold and U. Mosel, On QCD sum rules for vector mesons in nuclear medium, Phys. Rev. C **58**, 2939 (1998), arXiv:nucl-th/9805024.
- [34] S. Navas *et al.* (Particle Data Group), Review of particle physics, Phys. Rev. D **110**, 030001 (2024).
- [35] S. Bethke, The 2009 World Average of alpha(s), Eur. Phys. J. C **64**, 689 (2009), arXiv:0908.1135 [hep-ph].
- [36] Y. Aoki *et al.* (RBC, UKQCD), Continuum Limit Physics from 2+1 Flavor Domain Wall QCD, Phys. Rev. D **83**, 074508 (2011), arXiv:1011.0892 [hep-lat].
- [37] C. A. Dominguez, N. F. Nasrallah, and K. Schilcher, Strange quark condensate from QCD sum rules to five loops, JHEP **02**, 072, arXiv:0711.3962 [hep-ph].
- [38] A. Bazavov *et al.*, The chiral and deconfinement aspects of the QCD transition, Phys. Rev. D **85**, 054503 (2012), arXiv:1111.1710 [hep-lat].
- [39] O. Chabowski, J. I. Kapusta, and M. Singh, Relaxation times for disoriented isospin condensates in high energy heavy ion collisions, Phys. Rev. C **111**, 024903 (2025), [Erratum: Phys.Rev.C 112, 019902 (2025)], arXiv:2409.03711 [hep-ph].
- [40] S. Borsanyi, Z. Fodor, C. Hoelbling, S. D. Katz, S. Krieg, and K. K. Szabo, Full result for the QCD equation of state with 2+1 flavors, Phys. Lett. B **730**, 99 (2014), arXiv:1309.5258 [hep-lat].
- [41] P. Gubler and D. Satow, Recent Progress in QCD Con-

- densate Evaluations and Sum Rules, *Prog. Part. Nucl. Phys.* **106**, 1 (2019), arXiv:1812.00385 [hep-ph].
- [42] C. Alexandrou *et al.* (Extended Twisted Mass), Quark and Gluon Momentum Fractions in the Pion and in the Kaon, *Phys. Rev. Lett.* **134**, 131902 (2025), arXiv:2405.08529 [hep-lat].
- [43] J. C. Collins, A. Duncan, and S. D. Joglekar, Trace and Dilatation Anomalies in Gauge Theories, *Phys. Rev. D* **16**, 438 (1977).
- [44] N. K. Nielsen, The Energy Momentum Tensor in a Non-abelian Quark Gluon Theory, *Nucl. Phys. B* **120**, 212 (1977).
- [45] T. Hatsuda and T. Kunihiro, Strange quark, heavy quarks, and gluon contents of light hadrons, *Nucl. Phys. B* **387**, 715 (1992).
- [46] S. Borsanyi, G. Endrodi, Z. Fodor, A. Jakovac, S. D. Katz, S. Krieg, C. Ratti, and K. K. Szabo, The QCD equation of state with dynamical quarks, *JHEP* **11**, 077, arXiv:1007.2580 [hep-lat].
- [47] M. Gluck, E. Reya, and I. Schienbein, Pionic parton distributions revisited, *Eur. Phys. J. C* **10**, 313 (1999), arXiv:hep-ph/9903288.
- [48] M. A. Shifman, Snapshots of hadrons or the story of how the vacuum medium determines the properties of the classical mesons which are produced, live and die in the QCD vacuum, *Prog. Theor. Phys. Suppl.* **131**, 1 (1998), arXiv:hep-ph/9802214.